Song *et al. Molecular Cancer* (2025) 24:53
https://doi.org/10.1186/s12943-025-02261-6

Molecular Cancer

RESEARCH

Open Access

CircAKT3 promotes prostate cancer proliferation and metastasis by enhancing the binding of RPS27A and RPL11

Xiaoming Song[1†], Ziwei Wei[2†], Cong Zhang[3], Dunsheng Han[1], Jinke Liu[1], Yufeng Song[1], Xuefeng Xie[1], Dingchang Shao[1], Mingkun Zhao[1], Fan Chao[4], Guoxiong Xu[5*], Shiyu Wang[5*] and Gang Chen[1*]

Abstract

Background Metastatic prostate cancer (PCa) is a leading cause of mortality among PCa patients. Although circular RNAs (circRNAs) are recognized for their pivotal roles in tumorigenesis, the specifics of their influence within the context of PCa have yet to be fully elucidated.

Methods RT-qPCR was conducted to evaluate circAKT3 expression in PCa cells and in both tumor and adjacent non-cancerous tissues. The oncogenic role of circAKT3 was confirmed through a combination of in vitro and in vivo experiments. Mechanistic investigations using RNA-pulldown, RNA immunoprecipitation (RIP), fluorescence in situ hybridization (FISH), immunofluorescence (IF), and Chromatin Immunoprecipitation (ChIP) assays explored how circAKT3 modulates c-Myc activity via interactions with RPS27A and RPL11. Additionally, Western Blotting and further in vitro and in vivo studies assessed circAKT3's influence on PCa progression through MST1.

Results This research identified the function and regulation of circAKT3, a circRNA derived from exons 2 to 8 of the kinase-b3 (*AKT3*) gene, in human PCa cells. CircAKT3 was significantly correlated with clinical indicators of disease severity, including D'Amico risk classification, the Gleason score, and pT stage. Both in vitro and in vivo experiments demonstrated that circAKT3 knockdown inhibited PCa cell proliferation, migration, and invasion. Lipid nanoparticles encapsulating si-circAKT3 (LNP-si-circAKT3) effectively suppressed the growth of bone tumors formed by PCa cells. Mechanistically, circAKT3 acted as a protein scaffold between ribosomal protein S27a (RPS27A) and ribosomal protein L11 (RPL11), promoting their cytoplasmic translocation and reducing nuclear RPL11 levels, ultimately diminishing RPL11's interaction with c-Myc and resulting in enhanced c-Myc-driven suppression of macrophage stimulating 1 (MST1) expression. Consequently, the decreased MST1 led to PCa progression and metastasis. CircAKT3 formation was facilitated by both flanking Alu elements and the RNA binding protein Quaking (QKI). Additionally, downregulation of the RNA helicase URH49 resulted in the nuclear accumulation of circAKT3, finally suppressing MST1 expression.

†Xiaoming Song and Ziwei Wei contributed equally to this work.

*Correspondence:
Guoxiong Xu
guoxiong.xu@fudan.edu.cn
Shiyu Wang
sywang19@fudan.edu.cn
Gang Chen
chen_gang@fudan.edu.cn
Full list of author information is available at the end of the article

Conclusion Our findings suggest that circAKT3 acts as a protein scaffold, promoting the interaction between RPS27A and RPL11, thereby influencing c-Myc activity and PCa progression. This study underscores the crucial role of circAKT3 in PCa and its potential as a therapeutic target to impede malignancy progression and metastasis.

Keywords CircAKT3, RPS27A, RPL11, C-Myc, MST1, Prostate cancer

Introduction

Prostate cancer (PCa) is the most frequently diagnosed malignancy in men, with a global incidence that continues to rise, accounting for nearly 29% of newly diagnosed male cancers in 2024 [1]. While surgical intervention and radiotherapy provide effective treatment options for patients with localized PCa, in patients with advanced PCa, symptoms such as urinary difficulties, severe hematuria, and bone pain exert a profound negative impact on both the physiological and psychological well-being of the individuals. However, the treatment of advanced PCa remains a clinical challenge [2, 3]. Therefore, it is imperative to deeply explore the molecular mechanisms underlying PCa and to implement corresponding therapeutic strategies.

Circular RNAs (circRNAs) represent a unique class of covalently closed RNAs, characterized by their distinctive circular structure, which confers remarkable stability and resistance to RNase R digestion [4, 5]. CircRNAs are primarily formed via back-splicing, a process driven by complementary sequences in flanking introns. Alu elements, in particular, play a pivotal role in facilitating circRNA biogenesis [6, 7]. These molecules are primarily localized in the cytoplasm, although their formation occurs within the nucleus [7]. Previous studies have demonstrated that the absence of certain proteins, such as URH49, exportin-2, and Ran-GTP, can lead to the accumulation of circRNA in the cell nucleus [7, 8]. Functionally, circRNAs contribute to tumor progression and metastasis by interacting with RNA-binding proteins (RBPs). For example, circRNAs can bind to proteins to form circRNA-protein complexes, thereby modulating the biological functions of these proteins [9]. Moreover, circRNAs can act as scaffolds for protein–protein interactions, altering the functions of the associated proteins [10]. These multifaceted roles underscore the potential of circRNAs as both biomarkers and therapeutic targets in cancers [11–13].

Ribosomal protein S27a (RPS27A) plays a dual role in ribosome assembly and the ubiquitin–proteasome system [14]. Recent studies suggest that RPS27A may promote cancer progression through its interactions with other proteins or by modulating the expression of its host protein [15]. However, the exact regulatory mechanisms underlying these processes require further investigation. Ribosomal protein L11 (RPL11) not only suppresses tumor growth but also influences cancer invasion and metastasis by inhibiting c-Myc activity which is crucial within the RPL11/c-Myc axis [16, 17]. Extensive research has highlighted c-Myc as a primary oncogenic driver, and its inhibition has been shown to significantly curb tumor progression [18]. Macrophage stimulating 1 (MST1) plays a vital role in various cellular processes, including cell survival and migration. Recent studies indicate that tumor-associated mutant p53 represses MST1 gene expression, resulting in lower MST1 levels and increased resistance to apoptosis in cancer cells, thereby promoting oncogenesis [19].

In this study, circRNA-sequencing revealed that circAKT3 (hsa_circ_0017252) is significantly upregulated in PCa tissue and highly metastatic PCa cells. CircAKT3 is generated by back-splicing of seven exons (exons 2, 3, 4, 5, 6, 7, and 8) from the *AKT3* gene (AKT serine/threonine kinase 3). Functionally, circAKT3 acts as a molecular scaffold, enhancing the binding of RPS27A and RPL11, leading to the inhibition of their nuclear translocation. This inhibition prevents RPL11 from suppressing c-Myc in the nucleus, allowing c-Myc to bind to the MST1 promoter region and repress its transcription. This repression reduces MST1 mRNA and protein levels, thereby facilitating PCa progression. We identified that circAKT3 formation relies on flanking Alu elements and is regulated by the RNA binding protein Quaking (QKI). Furthermore, downregulation of the ATP-dependent RNA helicase URH49 leads to nuclear accumulation of circAKT3, further enhancing the c-Myc activity. Overall, this research unveils a novel regulatory role of circAKT3, revealing a new mechanism by which c-Myc drives PCa progression and metastasis.

Materials and methods

Tissue samples and cell lines

PCa and matched adjacent noncancerous prostate (ANP) tissues were collected from 50 patients at Jinshan Hospital, Fudan University, with diagnoses confirmed by two independent pathologists. The study received approval from the Ethics Committee of Jinshan Hospital, Fudan University, and written informed consent was obtained

from all patients. The cell lines used in this study were provided by the Fuheng Cell Center (Shanghai, China). PC-3 cells in DMEM/F12, DU145, BPH-1, and HEK293T cells in DMEM, and 22RV1 cells in RPMI 1640. 10% fetal bovine serum (FBS) was added to the culture medium. HLECs and HUVECs were cultured in endothelial cell medium (ECM) supplemented with 5% FBS and 5% Endothelial Cell Growth Supplement (ECGS). All cell lines were authenticated, tested for Mycoplasma contamination, and cultured at 37 ℃ with 5% CO_2. RNA could be extracted from 22Rv1 cells after 24 h of treatment with either enzalutamide (ENZA, Cat #: SC0074, Beyotime, Shanghai, China) or dihydrotestosterone (DHT, Cat #: D077, Sigma-Aldrich, USA). For protein extraction, cells should be cultured for 48 h under the same treatment conditions.

High-throughput circRNA-sequencing

High-throughput circRNA-sequencing was performed on highly metastatic (HM) and wild-type (WT) PC-3 cells [20]. Additionally, high-throughput circRNA-sequencing was conducted on three pairs of PCa and ANP tissue samples obtained from patients with neuroinvasive or bone metastases [21].

RNA extraction, nucleocytoplasmic fractionation, and real-time quantitative polymerase chain reaction (RT-qPCR)

Total RNA was extracted from cells using the RNA Rapid Purification Kit (Cat #: RN001, Yishan, Shanghai, China), while nuclear and cytoplasmic RNA fractions from PCa cells were isolated with the Cytoplasmic and Nuclear RNA Purification Kit (Cat #: 21000, Norgen Biotek, ON, Canada). RNA concentrations were measured, and RNA was subsequently reverse-transcribed into cDNA using the PrimeScript RT Master Mix (Cat #: RR036A, Takara, Shiga, Japan). RT-qPCR was performed with BeyoFast SYBR Green qPCR Mix (Cat #: D7262, Beyotime, Shanghai, China) on an ABI Quantstudio 3 real-time PCR system (Thermo Fisher Scientific, Waltham, USA). The primers used for amplification are listed in Table S1.

RNase R treatment

Total RNA from PCa cells were treated with RNase R (1 U/mg; Epicentre, USA) at 37 °C for 10 min, followed by a 10-min incubation at 70 °C to terminate the reaction. CircAKT3 and AKT3 mRNA levels were then quantified by RT-qPCR.

Actinomycin D (ACTD) treatment

ACTD (Cat #: 50–76-0, Sigma-Aldrich, USA) was added to the culture medium at a final concentration of 2 μg/mL. Cells were collected at designated time points, and circAKT3 and *AKT3* mRNA levels were quantified by RT-qPCR.

Plasmids and RNAi

To construct the circAKT3 overexpression plasmid, the full-length circAKT3 sequence, along with its flanking sequences that facilitate circularization, was inserted into the pLVX-IRES-Puro vector (Novopro, Shanghai, China). An empty vector was used as the control. SiRNAs of circAKT3 were designed, and the corresponding shRNAs were synthesized and cloned into vector PLKO.1 by GenePharma (Shanghai, China). The plasmids pLVX-IRES-Puro, pMD2.G, and pSPAX2 were co-transfected into HEK293T cells using LipoD293 transfection reagent (SignaGen Laboratories, Rockville, MD, USA) to generate lentivirus. Stably transfected cells were selected with puromycin. The sequences of the siRNA and shRNA are provided in Table S2.

Immunofluorescence (IF) and fluorescence in situ hybridization (FISH)

Cells were pre-plated on coverslips and allowed to adhere before fixation with 4% paraformaldehyde. Subsequently, they were incubated with the primary antibody overnight at 4 °C. The cells were then incubated with a fluorescently labeled secondary antibody at room temperature for 2 h. Following this, all cells were incubated overnight at 37 °C with a Cy5-labeled circAKT3 probe. Coverslips were mounted using a DAPI-containing mounting medium, and images were captured using a confocal microscope (Agilent, CA, USA). Details of the probes and antibodies are provided in Tables S3-4.

Migration, invasion, and trans-endothelial migration (TEM) assays

Migration and invasion assays were conducted as previously described [20, 22]. For the TEM model, HLEC or HUVEC were first seeded in the upper chamber (1×10^5 cells per well) and incubated for 24–48 h [23]. After the medium was removed from the upper chamber, GFP-labeled cells were then seeded into the upper chamber. Following incubation for a specified period, the migrated GFP-positive tumor cells in the lower chamber were imaged using a fluorescence microscope [24].

Wound-healing assay

The assay followed established protocols [22]. Upon reaching ~ 90% confluence in a six-well plate, a vertical scratch was made with a 200 μL pipette tip. Images were captured immediately (0 h), and cell migration into the scratch area was monitored and recorded after a set period (48 h for DU145, 24 h for PC-3) to assess migratory capacity.

CCK-8 assay and colony formation assay

Details of the CCK-8 assay and colony formation assay were as previously described [20]. In each well of a 96-well plate, 5 × 10^3 cells were seeded. Cell viability or proliferation was assessed every 24 h by adding CCK-8 reagent and measuring absorbance. For the IC_{50} experiment, 5 × 10^3 22Rv1 cells were seeded per well in a 96-well plate and incubated for 8 h to allow cell attachment. Afterward, 200 μL of culture medium containing varying concentrations of ENZA was added: 0.1, 10, 20, 40, 60, 100, and 150 μM. Cells were incubated for 48 h, followed by the addition of CCK-8 reagent. After a 2-h incubation at 37 °C, absorbance was measured at 450 nm using a microplate reader to assess cell viability. To evaluate proliferative and colony-forming capacity, individual cells were cultured until visible colonies formed, which were then stained with crystal violet for counting.

RNA-pulldown assay, liquid chromatography-tandem mass spectrometry (LC–MS/MS), and Western blotting

The 5'-biotin-labeled circAKT3 probe was synthesized by Genewiz (Suzhou, China). The procedure followed the instructions provided with the RNA-pulldown Kit (Cat #: 5102S, BerSinBio, Guangzhou, China). Briefly, the probe was incubated with cell lysates, and the probe-protein complexes were captured using streptavidin-coated magnetic beads. After thorough washing, the complexes were analyzed by LC–MS/MS. Western blotting analysis was carried out according to previously described methods [25]. Details of the probes and antibodies are provided in Tables S3-4.

RNA Immunoprecipitation (RIP) assay

The procedure was conducted according to the instructions provided with the BerSinBio RIP Kit (Cat #: 5101S, Guangzhou, China). In brief, anti-RPL11 (Cat #: 16,277-1-AP, Rosemont, USA), anti-RPS27A (Cat #: A2027, Wuhan, China), and anti-IgG antibodies were utilized to isolate RBPs and their associated RNA complexes from cell lysates. The co-precipitated RNA was subsequently detected by RT-qPCR. The catalog numbers for the antibodies are provided in Table S4.

Co-Immunoprecipitation (Co-IP) assay

The experiment was conducted using the BerSinBio Co-IP Kit (Cat #: 3011S, Guangzhou, China). Briefly, the target antibody was incubated with cell lysates overnight at 4 °C, followed by the binding of antibody-antigen complexes to Protein A/G magnetic beads. After washing and elution, protein interactions were analyzed by Western blotting. The catalog numbers for the antibodies are provided in Table S4.

Chromatin Immunoprecipitation (ChIP) assay

The experiment was conducted using the Chromatin IP Kit (Cat #: 9003, Cell Signaling Technology, USA). Briefly, cells were crosslinked with 1% formaldehyde at room temperature and then sonicated. The lysate was incubated overnight at 4 °C with anti-c-Myc antibody and anti-rabbit IgG antibody. Magnetic beads were subsequently added to the antibody-lysate mixture and incubated at 4 °C for 2 h. The mixture was then eluted, and DNA fragments were purified. Specific primers were used for RT-qPCR. Details of the primers and antibodies used are provided in Table S1 and Table S4.

(See figure on next page.)

Fig. 1 Characteristics of circAKT3 in prostate cancer. **A** CircRNA microarray analysis indicated that circAKT3 levels were higher in PCa tissues compared to ANP tissues. **B** High-throughput sequencing analysis revealed circAKT3 upregulation in HM PC-3 cells compared to WT PC-3 cells. **C** CircAKT3 was identified through two distinct circRNA sequencing analyses. **D** Schematic representation of circAKT3. **E** Sanger sequencing validated the sequences at the back-splice site of circAKT3. **F** CircAKT3 (808 bp) was amplified using both convergent primers (product: 106 bp) and divergent primers (product: 176 bp) in cDNA, but only with convergent primers in gDNA. **G-H** The expression levels of circAKT3 and *AKT3* mRNA in PCa cells were assessed with and without RNase R treatment or following actinomycin D treatment. Data are presented as mean ± SD. ***$P < 0.001$, Student's *t*-test, $n = 3$. **I** The abundance of circAKT3 in the cytoplasmic and nuclear fractions of PCa cells was analyzed using RT-qPCR, with β-actin serving as a positive control for the cytosol and NEAT1, a nuclear lncRNA, as the nuclear control. Data are presented as mean ± SD. **J** Subcellular localization of circAKT3 was determined using the RNA-FISH assay (red), with nuclei counterstained with DAPI (blue). Scale bar, 20 μm. **K** The expression levels of circAKT3 in benign prostatic hyperplasia epithelial cells (BPH-1) and PCa cell lines were analyzed via RT-qPCR. Data are presented as mean ± SD. ***$P < 0.001$, **$P < 0.01$, Student's *t*-test, $n = 3$. **L** The relative expression of circAKT3 in ANP and PCa tissues from 50 patients was analyzed using RT-qPCR. ***$P < 0.001$, Wilcoxon matched-pairs signed-rank test, $n = 50$ pairs. **M** The expression ratio of circAKT3 in ANP and PCa tissues of 50 patients

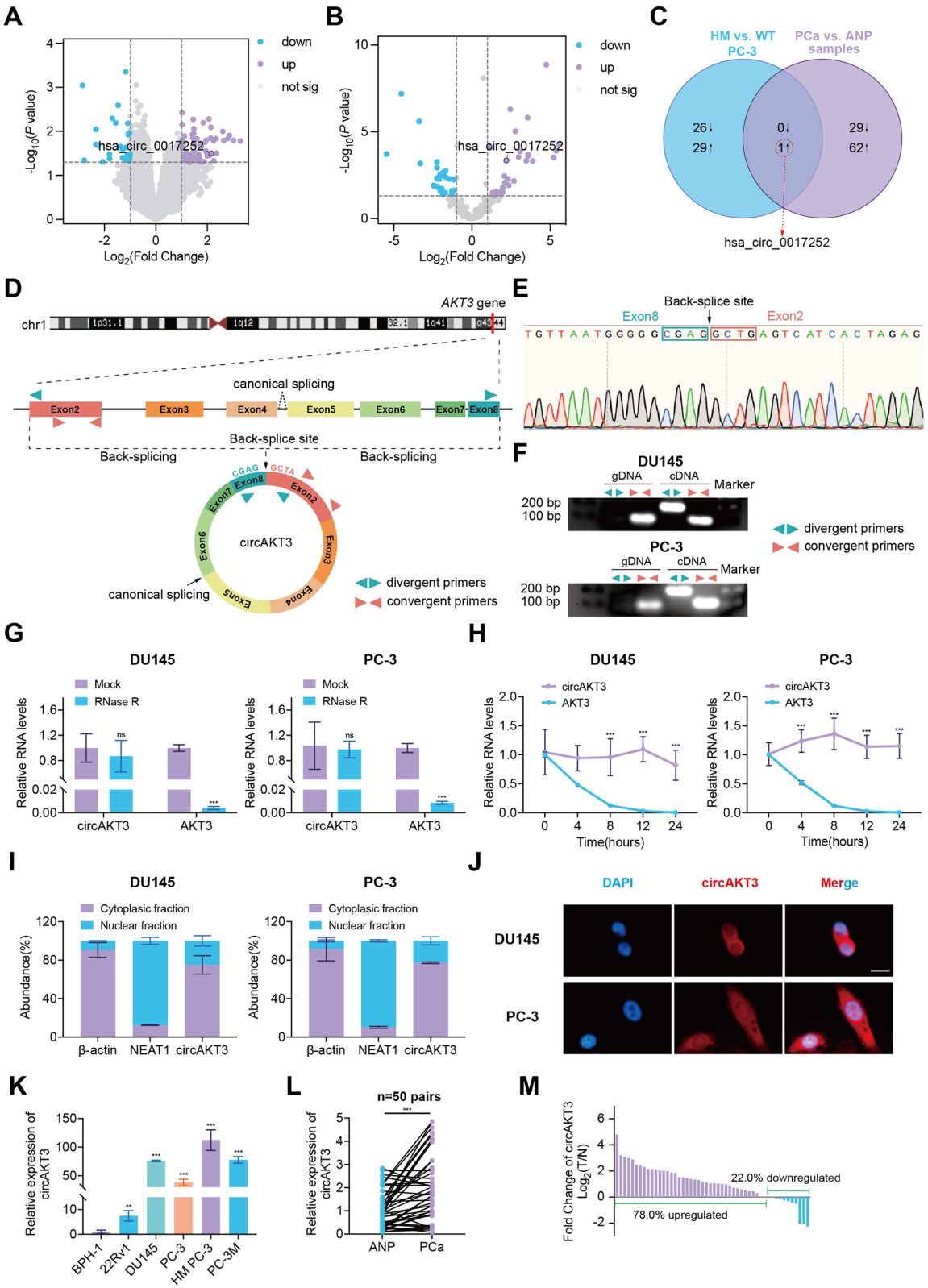

Fig. 1 (See legend on previous page.)

Table 1 Correlation between circAKT3 expression and clinical characteristics

Characteristic		Expression of circAKT3		*P* value
		High ($n=25$)	Low ($n=25$)	
(mean ± SD) age, years		(68.76 ± 6.67)	(67.20 ± 7.11)	0.428[a]
Median (IQR) PSA, ng/mL		13.08(9.41,26.08)	10.90(7.29,18.45)	0.116[b]
D'Amico risk classification n (%)	Low	0(0.0%)	3(6.0%)	0.003[c]
	Intermediate	7(14.0%)	15(30.0%)	
	High	18(36.0%)	7(14.0%)	
Total Gleason score n (%)	5	0(0.0%)	2(4.0%)	0.035[c]
	6	0(0.0%)	2(4.0%)	
	7	10(20.0%)	16(32.0%)	
	8	6(12.0%)	2(4.0%)	
	9	8(16.0%)	3(6.0%)	
	10	1(2.0%)	0(0.0%)	
pT stage n (%)	2	4(8.0%)	16(32.0%)	0.002[c]
	3	15(30.0%)	6(12.0%)	
	4	6(12.0%)	3(6.0%)	
pN stage n (%)	0	21(42.0%)	23(46.0%)	0.667[c]
	1	4(8.0%)	2(4.0%)	
pM stage n (%)	0	22(44.0%)	24(48.0%)	0.609[c]
	1	3(6.0%)	1(2.0%)	
Nerve invasion n (%)	No	10(20.0%)	16(32.0%)	0.156[c]
	Yes	15(30.0%)	9(18.0%)	

Gleason score, a grading system for prostate cancer. D'Amico risk classification, estimating the likelihood of recurrence

PCa prostate cancer, *ANP* adjacent noncancerous prostate, *IQR* interquartile range, *PSA* prostate-specific antigen

P[a]: Student's *t*-test

P[b]: wilcoxon rank-sum test

P[c]: chi-squared test

In vivo study

Tumor xenograft experiment

Five-week-old BALB/c-nu mice (Cat #: C201-01, SiPeiFu, Beijing, China) were randomly assigned into groups (6 mice per group). Mice were injected subcutaneously with 200 μL of 1×10^6 stable DU145 cells into the right dorsal flank. Tumor length and width were measured weekly, and tumor volume was calculated using the formula: $V=(length\times width^2)$ / 2. After 4 weeks, mice were euthanized, tumors were excised and weighed, and tumor tissues were prepared for H&E staining and immunohistochemistry.

Bone metastasis model

Mice were anesthetized, and their right ankle was externally rotated. Using a syringe inserted through the patella, 20 μL of 1×10^6 luc-PC-3 M cells were injected into the tibia [26]. After 2 weeks, LNP-si-ctrl (control) or Lipid nanoparticles encapsulating si-circAKT3 (LNP-si-circAKT3) was injected into the bone tumor tissues every three days, with 100 μL each time, for a total of 5 injections. In vivo imaging was conducted on days 14 and 30 post-injection. Mice were then euthanized, and tumor tissues were collected and stained.

(See figure on next page.)

Fig. 2 Downregulation of circAKT3 inhibits PCa cells proliferation, migration, and invasion both in vitro and in vivo. **A** RT-qPCR analysis of *AKT3* mRNA and circAKT3 expression in DU145, PC-3, and 22Rv1 cells transfected with circAKT3-specific siRNA or negative control siRNA. Data are presented as mean ± SD. ***$P<0.001$, **$P<0.01$, ns, not significant, Student's *t*-test, $n=3$. ctrl, control. **B** Colony formation assay revealed that circAKT3 knockdown reduced the proliferative ability of DU145, PC-3, and 22Rv1 cells. Data are presented as mean ± SD. ***$P<0.001$, **$P<0.01$, Student's *t*-test, $n=3$. **C** CCK-8 assay demonstrated that circAKT3 knockdown inhibited the proliferation of DU145, PC-3, and 22Rv1 cells. Data are presented as mean ± SD. ***$P<0.001$, Student's *t*-test, $n=3$. **D** Transwell assays indicated that circAKT3 knockdown reduced the migratory and invasive abilities of DU145, PC-3, and 22Rv1 cells. Scale bar, 100 μm. Data are presented as mean ± SD. ***$P<0.001$, Student's *t*-test, $n=3$. **E–F** Xenograft tumor models showed that tumors from the sh circ group were smaller than those from the sh ctrl group. **G-H**. Tumor volume changes over time and tumor weight after dissection.Data are presented as mean ± SD. ***$P<0.001$, Student's *t*-test, $n=6$

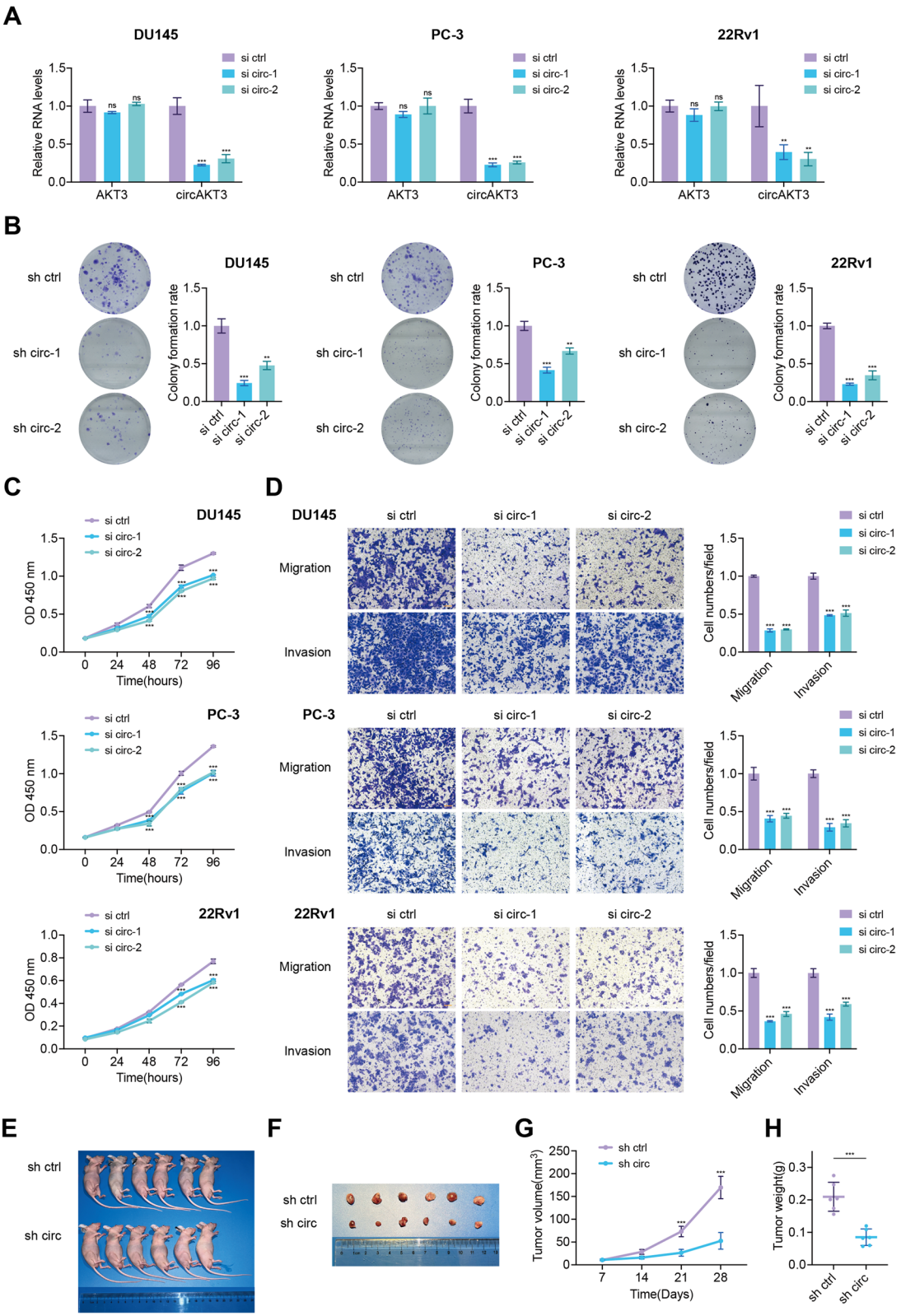

Fig. 2 (See legend on previous page.)

Statistical analysis

Data analysis was performed using Prism 9 (GraphPad Software, San Diego, USA). Statistical methods included Student's *t*-test, Wilcoxon rank-sum test, chi-square test, and Fisher's exact test. A p-value of ≤ 0.05 was considered statistically significant. PyMOL (Schrödinger, New York, NY, USA) was utilized to generate 3D molecular models.

Results

Characteristics of circAKT3 in PCa

To identify functional circRNAs, high-throughput circRNA-sequencing was performed on PCa and ANP tissues, as well as on HM and WT PC-3 cells. PCa and ANP tissues were obtained from three patients (Fig. 1A), while HM and WT PC-3 cells were selected from an in vitro model system (Fig. 1B). The sequencing results revealed a significant upregulation of circAKT3 (has_circ_0017252) in both PCa tissues and HM PC-3 cells compared to ANP and WT respectively, suggesting its potential role in advanced PCa (Fig. 1C). Database analysis (http://www.circbase.org) showed that circAKT3 is derived from exons 2 to 8 of the *AKT3* gene (Fig. 1D). The back-splice junction of circAKT3 was confirmed via Sanger sequencing (Fig. 1E). Gel electrophoresis demonstrated that only convergent primers produced a product in genomic DNA (gDNA), further verifying the circular nature of circAKT3 (Fig. 1F). We assessed circAKT3 and *AKT3* mRNA expression levels in PCa cells under various conditions, including RNase R treatment (to degrade linear RNA) and ACTD treatment, demonstrating the stability and circular structure of circAKT3 (Fig. 1G-H). Subcellular localization, determined through RT-qPCR and RNA-FISH assays, indicated that circAKT3 predominantly presented in the cytoplasm (Fig. 1I-J and S1A). Additionally, RT-qPCR analysis of benign prostatic hyperplasia epithelial cells (BPH-1) and multiple PCa cell lines confirmed circAKT3 upregulation, particularly in PCa and HM PC-3 cells (Fig. 1K). Furthermore, we analyzed circAKT3 expression in ANP and PCa tissues from 50 patients, revealing a marked elevation in cancerous compared to noncancerous tissues (Fig. 1L-M). Our analysis showed that high circAKT3 expression is positively correlated with D'Amico risk classification, the Gleason score, and pT stage, suggesting that circAKT3 plays a crucial role in the progression of PCa (Table 1).

CircAKT3 promotes PCa cell proliferation, migration, and invasion

The impact of circAKT3 knockdown on the proliferative, migratory, and invasive abilities of PCa cells was assessed in vitro. To achieve this, we designed two specific siRNAs targeting the back-splice site of circAKT3 as illustrated in Figure S2A. This approach was essential for efficiently silencing circAKT3. RT-qPCR confirmed the successful knockdown of circAKT3 without affecting *AKT3* mRNA levels in PCa cells transfected with circAKT3-specific siRNAs, compared to negative control siRNA (Fig. 2A). We next evaluated cell proliferation through CCK-8 and colony formation assays, which revealed that circAKT3 knockdown significantly inhibited the proliferation of DU145, PC-3, and 22Rv1 cells (Fig. 2B-C). Western blotting showed that circAKT3 knockdown reduced the expression of CDK4 protein, while simultaneously increasing the expression of the cyclin-dependent kinase inhibitors p21 and p27 (Fig. S2E-F). The migratory and invasive abilities of PCa cells were further assessed using Transwell and wound-healing assays. Results indicated that circAKT3 downregulation significantly reduced both cell migration and invasion (Figs. 2D and S2C). Additionally, Western blotting revealed a significant decrease in MMP9 expression after circAKT3 knockdown (Fig. S2G). To validate these in vitro findings in an in vivo model, we employed xenograft tumor models. Tumors derived from cells with circAKT3 knockdown were significantly smaller than those from control cells (Fig. 2E-F). Additionally, tumor volume was monitored over time, and tumor weight was measured after dissection. These results demonstrated that circAKT3 downregulation markedly suppressed tumor growth (Fig. 2G-H).

We next explored the effects of circAKT3 overexpression on PCa cells both in vitro and in vivo. A plasmid was constructed to achieve circAKT3 overexpression, as shown in Figure S2B. Despite the elevated levels of circAKT3, *AKT3* mRNA levels remained unchanged in the transfected cells, confirming that circAKT3 overexpression does not influence *AKT3* mRNA expression

(See figure on next page.)

Fig. 3 Overexpression of circAKT3 increases PCa cells proliferation, migration, and invasion in vitro and in vivo. **A** *AKT3* mRNA levels remained unchanged after circAKT3 overexpression in DU145, PC-3, and 22Rv1 cells stably transfected with plasmids. Data are presented as mean ± SD. ***$P < 0.001$, ns, not significant, Student's *t*-test, $n = 3$. **B-C** CCK-8 and colony formation assays demonstrated that circAKT3 overexpression enhanced PCa cells proliferation. Data are expressed as mean ± SD. ***$P < 0.001$, **$P < 0.01$, Student's *t*-test, $n = 3$. **D** Overexpression of circAKT3 enhanced PCa cells migration and invasion. Scale bar, 100 μm. Data are shown as mean ± SD. ***$P < 0.001$, Student's *t*-test, $n = 3$. **E–F** Xenograft tumor models indicated that tumors from the oe circ group were larger compared to those from the vector group. **G-H** Changes in tumor volume over time and tumor weight after dissection. Data are presented as mean ± SD. ***$P < 0.001$, Student's *t*-test, $n = 6$

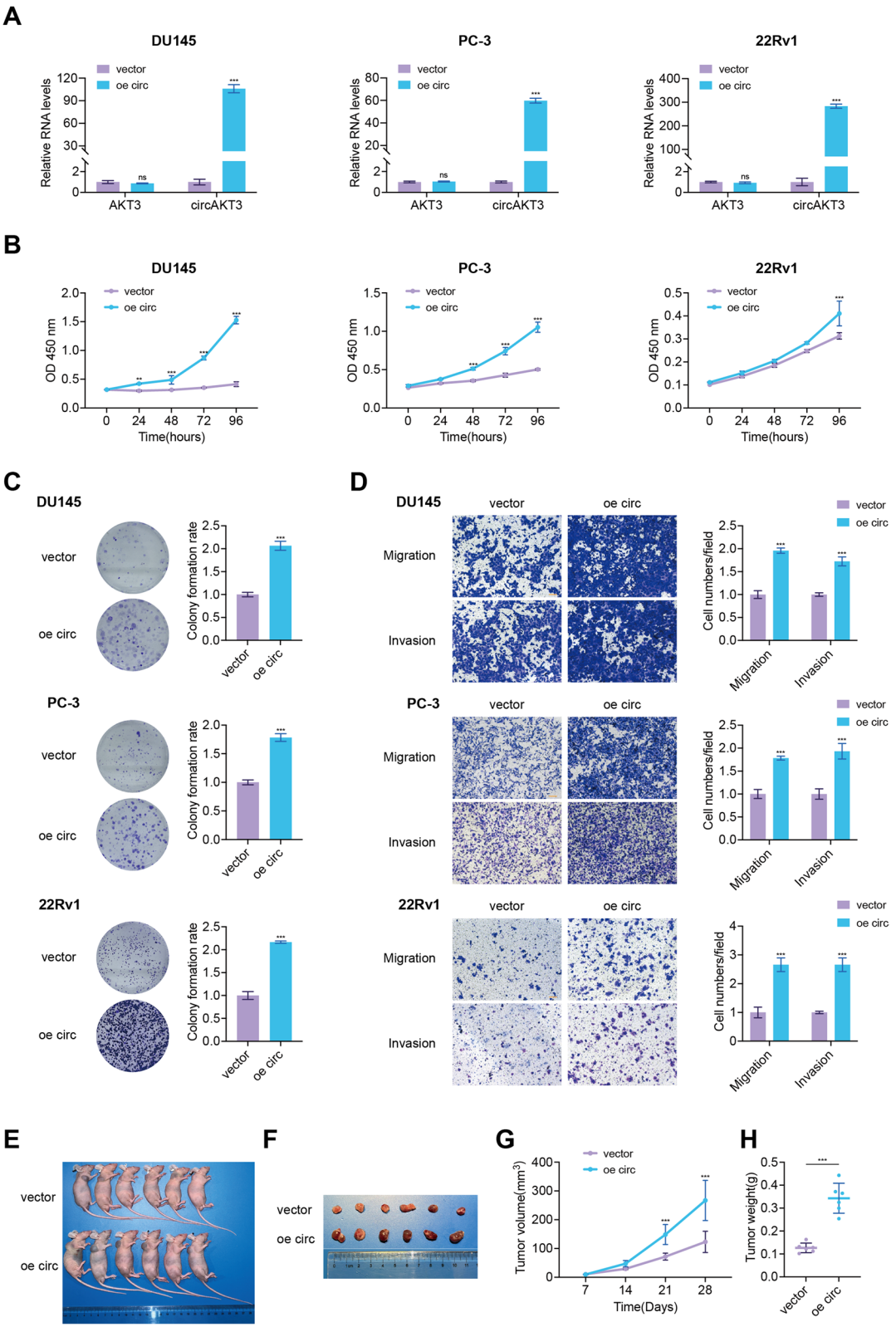

Fig. 3 (See legend on previous page.)

(Fig. 3A). In vitro assays demonstrated that circAKT3 overexpression significantly enhanced the proliferation, migration, and invasion of PCa cells (Figs. 3B-D and S2D). Similarly, in vivo experiments revealed that tumors generated from cells overexpressing circAKT3 were significantly larger than those in the control vector group (Fig. 3E-H), indicating that both knockdown and overexpression of circAKT3 respectively inhibit and promote PCa cell proliferation, migration, and invasion. These findings suggest that circAKT3 may act as an oncogenic driver in PCa progression.

CircAKT3 interacts with RPS27A and RPL11 to form a ternary complex, modulating their subcellular localization

To further investigate the mechanisms underlying circAKT3's biological functions, we used RNA-pulldown and LC–MS/MS assays, which identified specific amino acid sequences of RPS27A and RPL11, confirming their interactions with circAKT3 (Fig. 4A). Analysis of the TCGA database (https://portal.gdc.cancer.gov) revealed upregulation of both RPS27A and RPL11 in PCa, suggesting a potential association with cancer progression (Fig. S3A). To visualize the interaction and co-localization of circAKT3 with RPS27A and RPL11, we conducted FISH and IF analyses. These experiments produced both 2D and 3D images, which clearly showed the co-localization of these molecules within the cells (Fig. 4F and S3B). Using the RNAfold tool (http://rna.tbi.univie.ac.at/cgi-bin/RNAWebSuite/RNAfold.cgi), we predicted the secondary structure of circAKT3, providing insights into its structural properties that likely facilitate protein binding (Fig. S3C). Further validation of the interaction between circAKT3, RPS27A, and RPL11 was achieved via RNA-pulldown, followed by Western blotting, offering direct evidence of these protein interactions (Fig. 4B). RIP assay confirmed the specific binding of circAKT3 to both RPS27A and RPL11 (Fig. 4C). Additionally, Co-IP assays demonstrated that RPS27A and RPL11 interacted with each other, suggesting the formation of a ternary complex (Fig. 4D). To explore the role of circAKT3 in this interaction, we treated the complex with RNase A (which digests circAKT3) and observed a weakening of the RPS27A-RPL11 interaction (Fig. 4E). In contrast, RNase R treatment (which does not digest circAKT3) did not affect the interaction (Fig. S3D), highlighting the importance of circAKT3 in maintaining the stability of the complex. A simulation diagram illustrated the potential binding regions of RPS27A and RPL11 within circAKT3, along with a schematic of the ternary complex (Fig. 4G). Finally, Western blotting revealed increased nuclear levels of RPS27A and RPL11 in PCa cells following circAKT3 knockdown (Figs. 4H and S3E). IF assays further confirmed changes in the nuclear and cytosolic distribution of RPS27A and RPL11 in PCa cells transfected with circAKT3-specific siRNAs or circAKT3 overexpression plasmids (Figs. 4I and S3F), demonstrating that circAKT3 modulates the subcellular localization of RPS27A and RPL11, potentially affecting their cellular functions and contributing to PCa progression.

CircAKT3 modulates MST1 expression by enhancing the interaction between RPL11 and c-Myc

As previously reported, RPL11 inhibits the oncogenic effects of c-Myc by directly binding to c-Myc in the nucleus [16, 17]. To investigate this interaction, we performed a Co-IP analysis, which demonstrated that circAKT3 downregulation enhanced the interaction between RPL11 and c-Myc (Fig. 5A). Conversely, when circAKT3 was upregulated, the binding between RPL11 and RPS27A was strengthened, which in turn reduced the interaction between RPL11 and c-Myc (Fig. S4A). Further, Co-IP experiments confirmed the interaction between RPL11 and c-Myc, while no direct interaction was observed between RPS27A and c-Myc (Fig. S4B-C). These results suggested that circAKT3 indirectly modulated the RPL11-c-Myc interaction by influencing the formation of the RPL11-RPS27A complex.

(See figure on next page.)

Fig. 4 CircAKT3 interacts with RPS27A and RPL11 to form a ternary complex, inhibiting the nuclear translocation of both proteins. **A** Schematic overview of the RPD and LC–MS/MS assays (top). The specific amino acid sequences of RPS27A and RPL11 are depicted by the second-order mass spectrum (right). Data are presented as mean ± SD. ***$P < 0.001$, Student's *t*-test, $n = 3$. **B** The interaction between circAKT3, RPS27A, and RPL11 was confirmed using RPD followed by Western blotting. **C** A RIP assay validated the binding of circAKT3 to RPS27A and RPL11. Data are presented as mean ± SD. **$P < 0.01$, *$P < 0.05$, Student's *t*-test, $n = 3$. **D** A Co-IP assay demonstrated that RPS27A and RPL11 could interact with each other. **E** The interaction between RPS27A and RPL11 weakened after circAKT3 was digested with RNase A. **F** FISH and IF images revealed the co-localization of circAKT3, RPS27A, and RPL11 (scale bar, 20 μm). **G** Simulation diagram of the ternary complexes formed by circAKT3, RPS27A, and RPL11 (left). Schematic representation of the potential binding regions of RPS27A and RPL11 within circAKT3 (right). **H** Western blotting analysis of RPS27A and RPL11 in PCa cells transfected with negative control siRNA or circAKT3-specific siRNA. β-actin served as the loading control for the cytosol and lysis, and Lamin B1 for the nucleus. Data are presented as mean ± SD. ns, not significant; ***$P < 0.001$, **$P < 0.01$, *$P < 0.05$, Student's *t*-test, $n = 3$ independent experiments. **I** IF assays showed a significant increase in nuclear levels of RPS27A and RPL11 upon circAKT3 downregulation. Nuclei were counterstained with DAPI. Scale bar, 20 μm

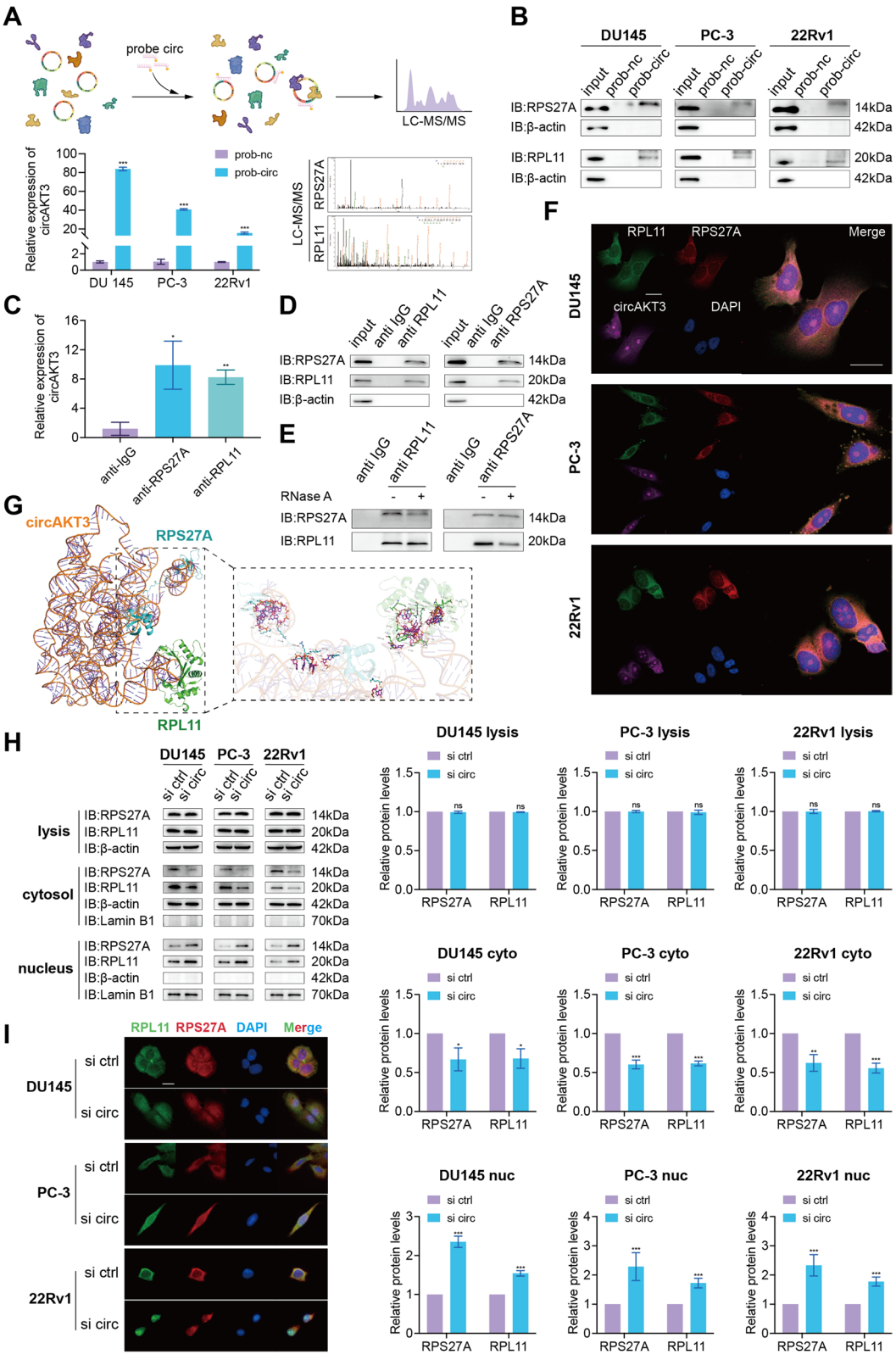

Fig. 4 (See legend on previous page.)

As shown in Figure S4D-E, changes in circAKT3 expression influenced the function of c-Myc without affecting its expression levels. Furthermore, the knockdown of circAKT3 also resulted in a reduction in p-ERK expression. To further investigate the downstream target genes regulated by both circAKT3 and c-Myc in PCa cells, we conducted an RNA-seq analysis in cells transfected with either si circAKT3 or si c-Myc (Fig. 5B). This analysis identified MST1 as the sole gene whose RNA levels were modulated by circAKT3 across multiple PCa cell lines, including DU145, PC-3, and 22Rv1 (Figs. 5C and S4F-G). Further, the protein levels of MST1 were found to increase in response to circAKT3 knockdown and decrease in response to circAKT3 overexpression (Fig. S4H).

Analysis of the TCGA database revealed a downregulation of MST1 in PCa (Fig. S5A). Compared to DU145 and PC-3 cells, MST1 was highly expressed in 22Rv1 cells (Fig. S5B-C). However, androgen stimulation led to a reduction in MST1 expression in 22Rv1 cells (Fig. S5D-E). After MST1 was successfully overexpressed (Figs. 5D-E and S5F), its effect on the proliferation of DU145, PC-3, and 22Rv1 cells was evaluated using CCK-8 and colony formation assays (Figs. 5F-G and S5G-H), which revealed that MST1 overexpression significantly inhibited the proliferation of PCa cells. Additionally, Transwell and Wound-healing assays demonstrated that MST1 overexpression inhibited the migratory and invasive abilities of PCa cells (Figs. 5H and S5I-J). In in vivo studies using xenograft tumor models, tumors from the MST1 overexpression group were smaller than those in the control (vector) group (Fig. 5I-J). Representative IHC staining images of MST1 in tumor xenografts are shown in Fig. 5M, while tumor volume progression and final tumor weights are presented in Fig. 5K-L, highlighting that MST1 overexpression markedly suppressed tumor growth. Supplementary Figure S6 details the effects of MST1 knockdown on PCa cell proliferation, migration, and invasion, both in vitro and in vivo. Specifically, after MST1 knockdown (Fig. S6A-B), PCa cell proliferation was promoted in both in vitro and in vivo models (Fig. S6C-D and S6F-J), and cell migration and invasion were enhanced (Fig. S5K and S6E).

These findings suggest that MST1 functions as a tumor suppressor in PCa. Our results demonstrated that circAKT3 regulates MST1 expression by modulating the interaction between RPL11 and c-Myc, thereby affecting the proliferation, migration, and invasion of PCa cells.

Potential c-Myc binding sites on the MST1 promoters

We further explored the regulatory mechanisms by which c-Myc could modulate MST1 expression in PCa cells, focusing on the identification of potential c-Myc binding sites on the MST1 promoters. Using the JASPAR database [27], we predicted possible c-Myc binding sites on the MST1 promoters, which are crucial for gene transcription regulation (Fig. 5N). The Transcription Start Site (TSS) served as a reference point for these predictions. Next, we performed ChIP-qPCR to assess the binding preference of c-Myc among the predicted sites. The results indicated that c-Myc may have a preferential binding to the third promoter region, designated as B3 (Figs. 5O and S7A). To further validate the sequences of the B3 binding site's RT-qPCR products, Sanger sequencing was employed, directly confirming the nucleotide sequences and ensuring the accuracy of our findings (Fig. 5P). Furthermore, the specificity of c-Myc binding to the B3 site of the MST1 promoter was further confirmed by demonstrating the absence of interaction with the non-binding site (NBS) (Fig. S7B-C). These results provide evidence for the direct regulation of MST1 by c-Myc via specific binding sites on the MST1 promoters, underscoring the critical role of transcription factors like c-Myc in gene expression modulation.

(See figure on next page.)

Fig. 5 CircAKT3 modulates MST1 expression by enhancing the interaction between RPL11 and c-Myc. **A** Co-IP analysis demonstrated that the interaction between RPL11 and c-Myc was strengthened when the binding of RPL11 and RPS27A was inhibited by circAKT3 downregulation. **B** Venn diagram illustrating potential target genes regulated by circAKT3 based on RNA-seq data from si circAKT3 and si c-Myc experiments. **C** MST1 was the only gene whose RNA levels were regulated by circAKT3 in DU145, PC-3, and 22Rv1 cells. Data are presented as mean ± SD. ***$P < 0.001$, **$P < 0.01$, *$P < 0.05$, ns, not significant, Student's *t*-test, $n = 3$. **D** MST1 protein levels were elevated after transfection with an MST1 overexpression plasmid. Data are presented as mean ± SD. **$P < 0.01$, Student's *t*-test, $n = 3$. **E** RT-qPCR analysis of *MST1* mRNA in 22Rv1 cells following plasmid transfection. Data are expressed as mean ± SD. ***$P < 0.001$, Student's *t*-test, $n = 3$. **F-G** CCK-8 and colony formation assays showed that overexpression of MST1 inhibited the proliferation of 22Rv1. Data are presented as mean ± SD. ***$P < 0.001$, Student's *t*-test, $n = 3$. **H** Transwell assays showed that MST1 overexpression decreased the migratory and invasive capacities of 22Rv1. Scale bar, 100 μm. Data are presented as mean ± SD. ***$P < 0.001$, Student's *t*-test, $n = 3$. **I-J** Xenograft tumor models indicated that tumors in the MST1 overexpression group were smaller compared to those in the vector group. **K-L** Tumor volume progression over time and tumor weight after dissection. Data are presented as mean ± SD. ***$P < 0.001$, **$P < 0.01$, Student's *t*-test, $n = 6$. **M**. Representative IHC staining images of MST1 in tumor xenografts. Scale bar = 100 μm. **N** The JASPAR database predicted potential c-Myc binding sites on the MST1 promoters. TSS: Transcription Start Site. **O** Gel electrophoresis was conducted to confirm the specificity of the RT-qPCR products. Data are presented as mean ± SD. ***$P < 0.001$, ns, not significant, Student's *t*-test, $n = 3$. **P** Sanger sequencing validated the sequences of B3's RT-qPCR products

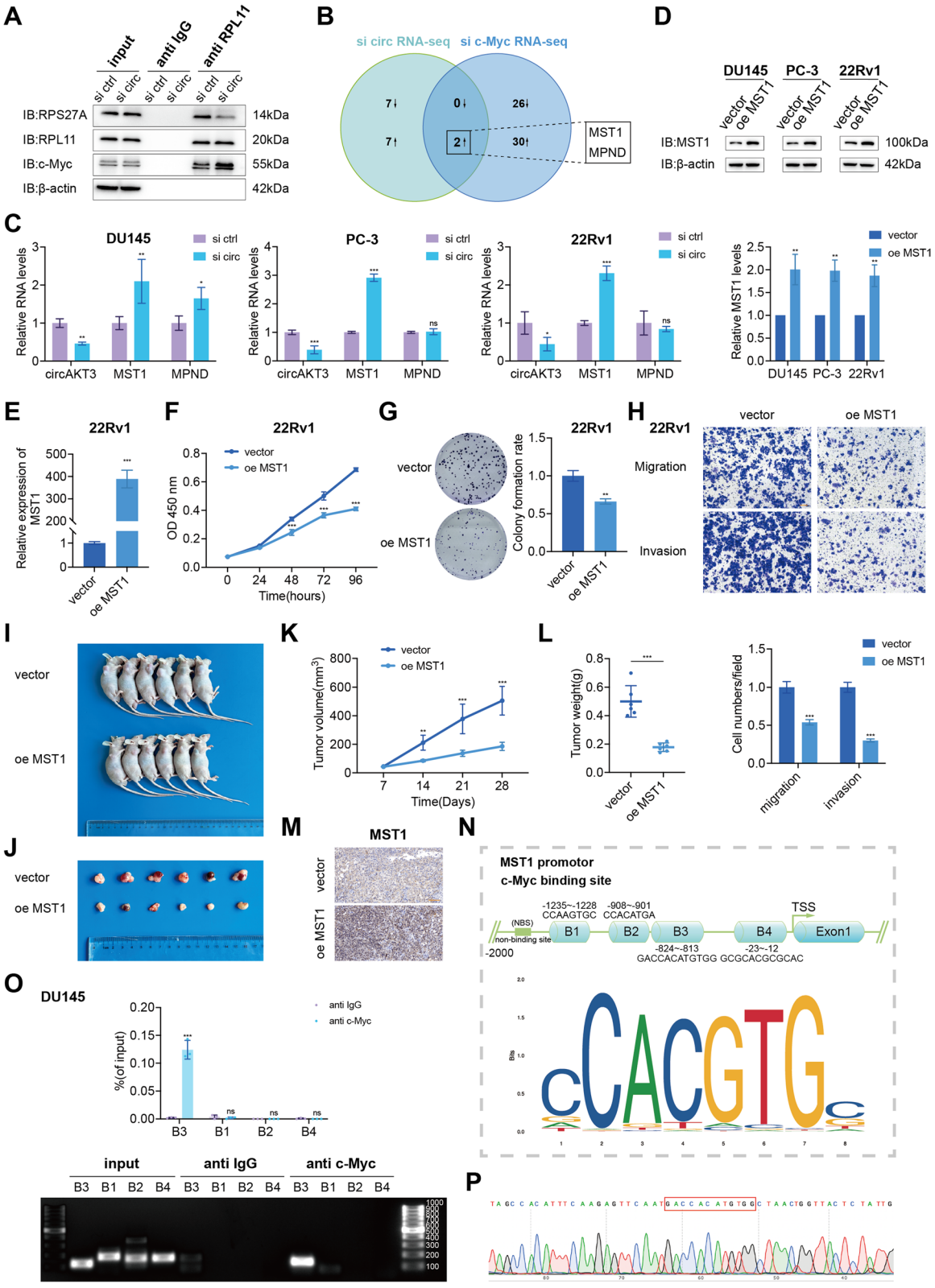

Fig. 5 (See legend on previous page.)

MST1 upregulation reversed the proliferative, migratory, and metastatic characteristics induced by circAKT3

We investigated the impact of MST1 upregulation in circAKT3-overexpressing PCa cells, particularly its effects on cell proliferation, migration, and invasion. Western blotting was initially conducted to assess MST1 expression levels in DU145, PC-3, and 22Rv1 cells transfected with various plasmids (Figs. 6A and S8A). Subsequently, colony formation and CCK-8 assays demonstrated that MST1 reversed the effects of circAKT3 overexpression on cell proliferation (Figs. 6B and S8B). Transwell assays, TEM assays, and wound-healing assays were further performed to evaluate the migratory and invasive abilities of the cells. The results indicated that MST1 upregulation effectively counteracted the increased migration and invasion induced by circAKT3 overexpression in PCa cells (Figs. 6C-D and S8C). In vivo studies corroborated the impact of MST1 upregulation on the proliferation of circAKT3-overexpressing cells, showing that MST1 overexpression mitigated the proliferation enhancement caused by circAKT3 overexpression (Fig. 6E-I). Additionally, we examined the effects of MST1 knockdown in circAKT3-knockdown PCa cells. Western blotting evaluated the efficiency of MST1 knockdown in DU145, PC-3, and 22Rv1 cells transfected with different constructs (Fig. S9A and S10A). The findings revealed that MST1 knockdown reversed the inhibitory effects of circAKT3 downregulation on cell proliferation, migration, and invasion (Fig. S9B-C and S10B-C).

Nucleic acid-based therapies, such as gene silencing, therapeutic protein expression, and gene editing, are rapidly advancing into clinical trials. Delivery of siRNA, mRNA, and DNA plasmids via LNP enables targeted in vivo treatment, significantly reducing systemic toxicity while maintaining therapeutic efficacy [28, 29]. In our study, we first established a mouse tumor xenograft model and administered LNP-si-ctrl or LNP-si-circAKT3, observing that LNP-si-circAKT3 markedly inhibited tumor growth (Fig. 7A-F). Figure 7G-H demonstrated that the knockdown of circAKT3 decreased the IC_{50} of ENZA in 22Rv1 cells. Given the lack of effective treatments for metastatic PCa, particularly for bone metastases, we hypothesized that LNP-si-circAKT3 could offer therapeutic potential in this setting. To test this, we developed a bone metastasis model by injecting PCa cells into the tibia to simulate the tumor growth in bone after PCa cell transplantation. Treatment with LNP-si-circAKT3 in this model led to significant tumor remission in the bone (Fig. 7I-M). These findings suggest a novel approach for treating metastatic PCa by combining circRNA with LNP-based delivery systems.

The circularization and nuclear export of circAKT3

To investigate the role of these flanking introns in the generation of circAKT3, we engineered four distinct plasmids (#1–#4) (Fig. 8A). Our results indicated that only plasmid #1 effectively promoted the circularization of circAKT3, suggesting a specific role for the flanking introns within this plasmid in the circularization process. Given the critical role of Alu sequences in circRNA circularization, we utilized the UCSC Genome Browser and BLAST to identify potential Alu sequences located in the flanking introns of circAKT3 (Fig. S11A-B). We identified AluSc and AluSx4 sequences. Notably, the deletion of these sequences in plasmid #5 resulted in inefficient circularization, underscoring their importance (Fig. 8B). Further experiments revealed that the presence of the AluSc and AluSx4 sequences (#6), rather than the entire 1000 bp flanking intron, was sufficient to significantly enhance the biogenesis of circAKT3 (Fig. 8C). Additionally, these sequences were found to promote the circularization of other circRNAs, such as circSOBP and circUBE3A (Fig. 8D). RBPs such as QKI, FUS, and hnRNPH1 have been reported to promote circRNA biogenesis [30]. Our results indicated that the knockdown of QKI affected the circularization of circAKT3, implicating it in the regulation of its biogenesis (Fig. S11C). Furthermore, circRNAs generated in the nucleus are exported out with the assistance of proteins such as URH49, exportin-2, and Ran-GTP [7, 8]. We examined the role of URH49 in the nuclear export of circAKT3. A reduction in URH49 expression (Figs. 8E and S11D) resulted in a

(See figure on next page.)

Fig. 6 MST1 upregulation reverses the proliferative, migratory, and metastatic characteristics induced by circAKT3. **A** Western blot analysis was conducted to evaluate MST1 expression in DU145, PC-3, and 22Rv1 cells harboring different vectors. Data are presented as mean ± SD. ***$P < 0.001$, ns, not significant, Student's *t*-test, $n = 3$. **B** Colony formation assays assessed cell mobility in cells with different vectors. Data are presented as mean ± SD. ***$P < 0.001$, ns, not significant, Student's *t*-test, $n = 3$. **C-D** Transwell assays (B; top; scale bar, 100 μm), transendothelial migration (TEM) assays (B; bottom; scale bar, 100 μm), and wound-healing assays (C; scale bar, 200 μm) demonstrated that upregulating MST1 in circAKT3-overexpressing PCa cells counteracted the migration and invasion enhancement driven by circAKT3 overexpression. Data are presented as mean ± SD. ***$P < 0.001$, ns, not significant, Student's *t*-test, $n = 3$. **E–F** Xenograft tumor models revealed that MST1 overexpression mitigated the proliferation boost caused by circAKT3 overexpression in vivo. **G**. Representative IHC staining of MST1 in tumor xenografts. Scale bar = 100 μm. **H-I** Tumor volume progression and tumor weight following dissection. Data are presented as mean ± SD. ***$P < 0.001$, *$P < 0.05$, ns, not significant, Student's *t*-test, $n = 6$

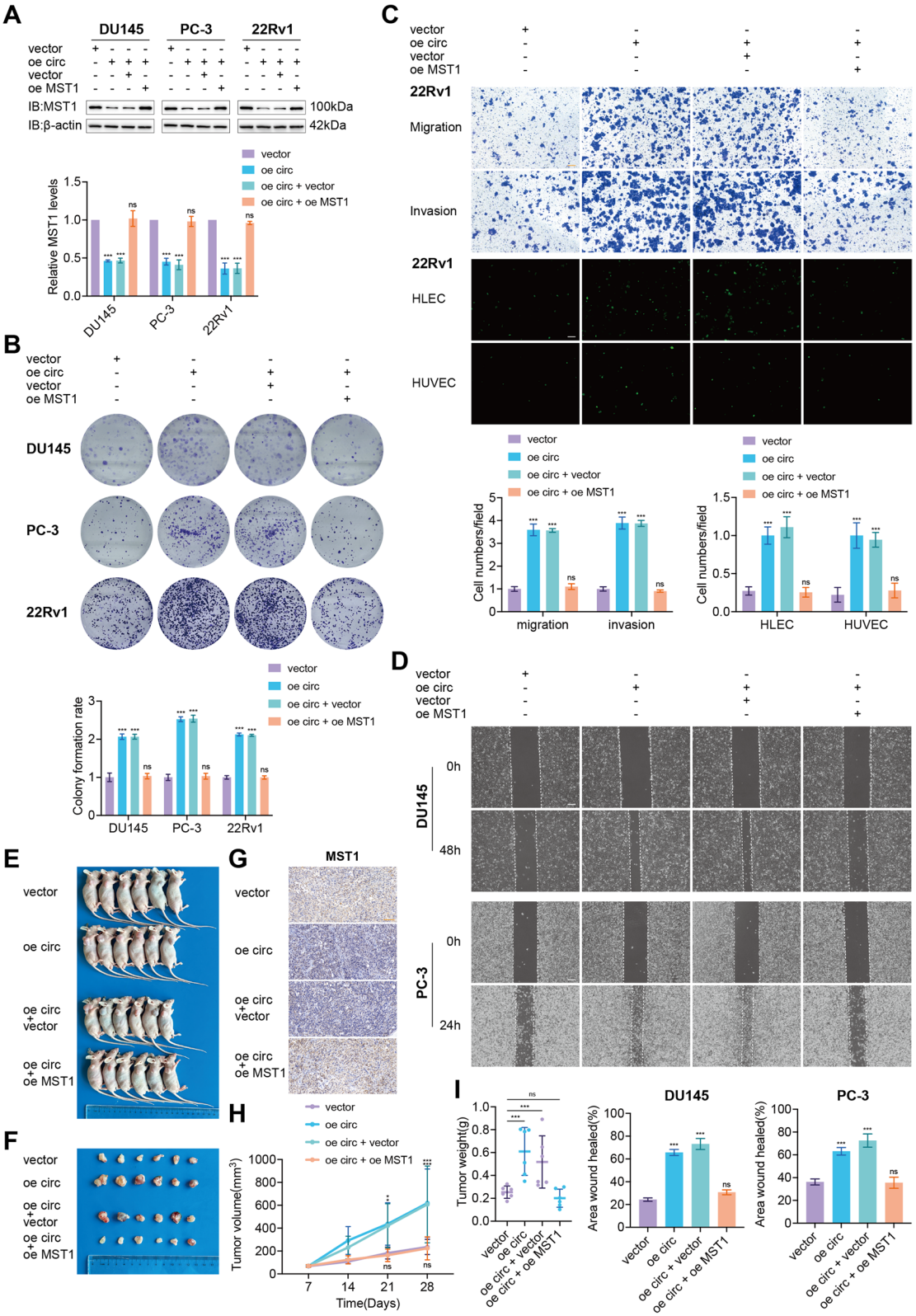

Fig. 6 (See legend on previous page.)

significant increase in the nuclear levels of circAKT3, as visualized by FISH (Fig. 8F) and quantified by RT-qPCR (Fig. 8G). Moreover, the downregulation of URH49 specifically decreased the levels of MST1 RNA in DU145 and PC-3 cells (Figs. 8H and Fig. S11E). These results suggest that the circularization of circAKT3 is driven by specific Alu sequences and the RNA-binding protein QKI, while its nuclear export is regulated by URH49.

Discussion

Metastatic PCa spreading via direct invasion, lymphatics, or the bloodstream leading to hematuria, lower limb edema, or severe bone pain, is frequently associated with poor prognosis [2]. Elucidating the molecular mechanisms driving PCa metastasis and identifying potential therapeutic targets are critical for improving treatment strategies [31, 32]. Emerging evidence suggests a link between circRNAs and cancer [13, 33]. Using high-throughput circRNA-sequencing, we identified circAKT3 as significantly upregulated in PCa, correlating with disease aggressiveness. Further analysis of circAKT3 expression alongside clinical-pathological data showed that higher circAKT3 levels are associated with D'Amico risk classification, the Gleason score, and pT stage, underscoring its potential as a prognostic marker. CircAKT3 originates from exons 2–8 of the *AKT3* gene, and its in vitro functional assays demonstrate its role in promoting PCa cell proliferation, migration, and invasion.

CircRNAs have been shown to regulate parental gene expression, act as "miRNA sponges", form circRNA-protein complexes, or encode peptides [5, 34]. Previous studies identified that circAKT3 functions as a sponge for miR-296-3p and miR-17-5p [35, 36]. To explore additional regulatory mechanisms, we first assessed whether circAKT3 affects its parental gene, *AKT3*, and found that neither circAKT3 knockdown nor overexpression altered *AKT3* expression. CircRNAs also interact with proteins, functioning as sponges, decoys, scaffolds, or recruiters [7]. Through RNA-pulldown and LC–MS/MS analysis, we identified circAKT3 binding to both RPS27A and RPL11. While earlier studies have reported the interaction between RPS27A and RPL11 [37], our research is the first to uncover the formation of a RPS27A-circAKT3-RPL11 ternary complex. Based on these findings, we hypothesized that circAKT3 serves as a scaffold facilitating this interaction. Interestingly, the digestion of circAKT3 with RNase A, but not RNase R, weakened the interaction between RPS27A and RPL11. Furthermore, circAKT3 knockdown reduced the interaction between RPS27A and RPL11 while promoting their nuclear translocation, resulting in increased nuclear accumulation of both proteins. To investigate the binding mechanism, we employed AlphaFold3 (https://alphafoldserver.com) and PyMOL to model and visualize the 3D structure of the RPS27A-circAKT3-RPL11 ternary complex [38], with the binding sites between circAKT3 and these proteins highlighted (Fig. 4G). CircRNAs interact with proteins in different ways as scaffolds: (a) by binding to two proteins and enhancing their interaction; (b) by binding to protein X and indirectly promoting its interaction with protein Y, without binding directly to protein Y; (c) by binding to two proteins that do not interact with each other. The formation of protein-circRNA-protein ternary complexes not only regulates the translocation of these proteins but also influences their functions by enhancing, sequestering, or modulating their activity and expression levels [39–41]. Based on our current findings, the RPS27A-circAKT3-RPL11 ternary complex aligns with the third mode of binding.

Studies have highlighted that nuclear RPL11 binds to c-Myc, inhibiting its transcriptional activity [16, 17]. Notably, circAKT3 knockdown not only promoted the nuclear translocation of RPS27A and RPL11 but, as shown by Co-IP analysis, also enhanced the binding between RPL11 and c-Myc while weakening the association between RPL11 and RPS27A. Additionally, circAKT3 knockdown decreased p-ERK expression, suggesting its involvement in PCa progression through the MAPK signaling pathway. Given that circAKT3 knockdown led to RPL11-mediated suppression of c-Myc transcriptional activity, we analyzed RNA-seq data from si circAKT3 and si c-Myc samples, coupled with cellular

(See figure on next page.)

Fig. 7 CircAKT3 inhibits PCa cells proliferation and metastasis in vivo. **A** Schematic illustration of the tumor xenograft experiment. **B-C** Xenograft tumor models showing that tumors from the LNP-si-circ group were smaller compared to those from the LNP-si-ctrl group. circ, circAKT3. ctrl, control. **D-E** Tumor volume changes over time and tumor weight post-dissection. Data are presented as mean ± SD. ***$P < 0.001$, *$P < 0.05$, Student's *t*-test, $n = 5$. **F** Representative IHC staining of MST1 in tumor xenografts. Scale bar = 100 μm. **G-H** Cell viability and relative IC_{50} values were assessed following knockdown of circAKT3 and treatment with ENZA in 22Rv1 cells. Data are expressed as mean ± SD. **$P < 0.01$, *$P < 0.05$, Student's *t*-test, $n = 3$ independent experiments. **I** Schematic representation of the bone metastasis model. **J** In vivo imaging and gross images of mouse legs from the bone metastasis model. **K** Hematoxylin and eosin (HE) staining of leg tissues. HE staining of normal leg tissue (Top). HE staining of tumor-affected leg tissue, with the red box indicating osteoclasts and the blue box indicating osteoblasts (Bottom). Scale bar = 500 μm, Scale bar = 50 μm. **L-M** Tartrate-resistant acid phosphatase (TRAP), red coloration indicates the presence of osteoclasts. Scale bar = 500 μm, Scale bar = 50 μm

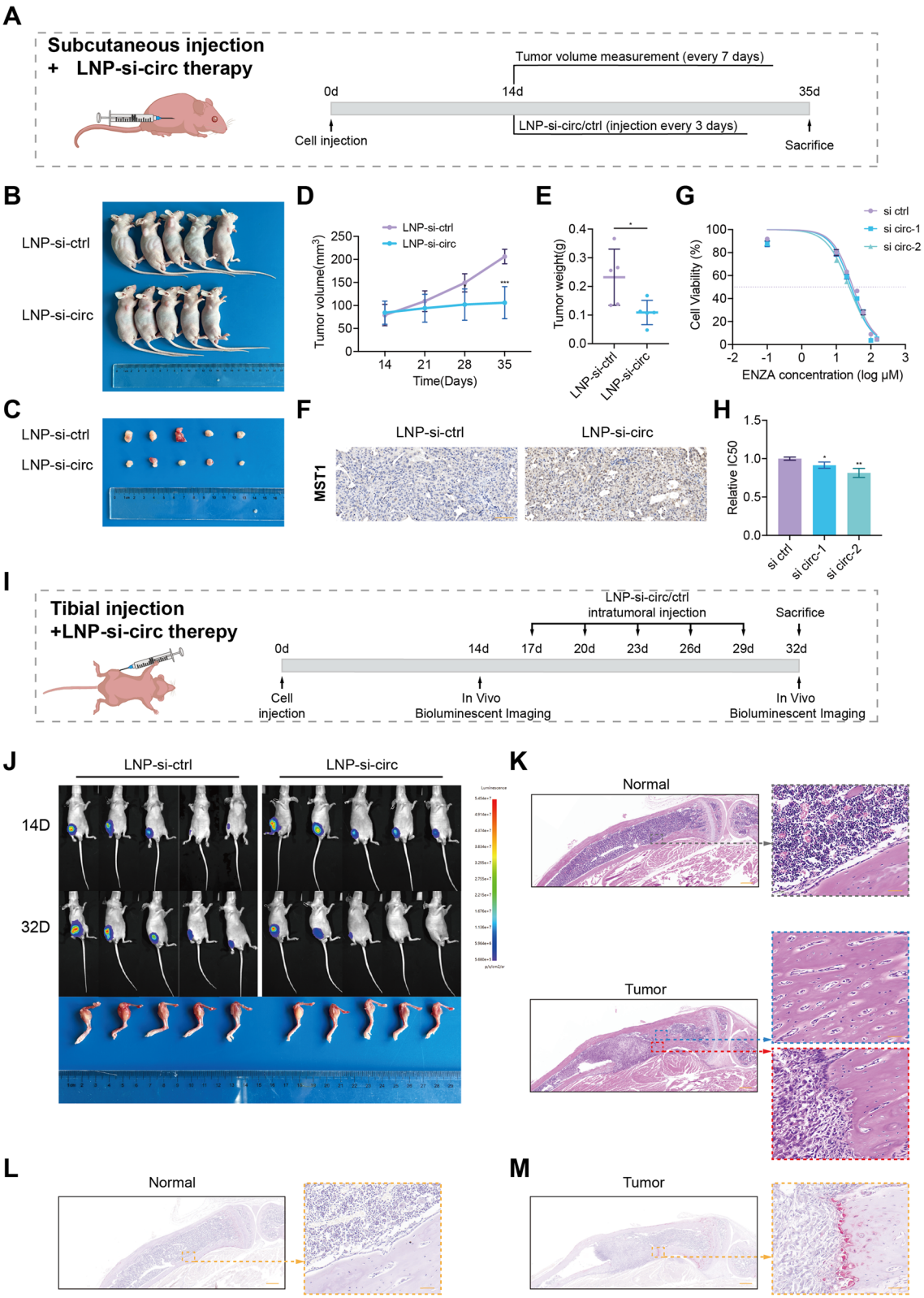

Fig. 7 (See legend on previous page.)

experiments, and identified MST1 as a potential downstream effector.

While some evidence suggests that MST1 contributes to tumor progression in extrahepatic cholangiocarcinoma and breast cancer [42, 43], other findings indicate that MST1 downregulation may promote tumorigenesis in lung carcinoma [19]. In PCa, previous studies have explored the relationship between plasma MST1 levels and clinicopathological features [44]. By analyzing plasma MST1 levels in 58 PCa patients, researchers found that Japanese patients with castration-resistant PCa (CRPC) exhibited higher MST1 levels compared to those with typical PCa. However, this study did not explore the role of MST1 in PCa cells' phenotypes. In our investigation, analysis of the TCGA database revealed that MST1 is expressed at low levels in PCa patients. Culturing androgen receptor-positive 22Rv1 cells in androgen-containing medium suppressed MST1 expression, while treatment with ENZA increased MST1 levels, suggesting a link between MST1 and androgen signaling. Notably, circAKT3 knockdown in 22Rv1 cells led to an increase in MST1 expression and simultaneously decreased the IC_{50} of ENZA. These findings suggested that MST1 expression was associated with the sensitivity of androgen receptor-positive 22Rv1 cells to ENZA treatment. In this study, we focus on in vitro and in vivo experiments, demonstrating that MST1 upregulation suppresses PCa cell proliferation, migration, and invasion. Moreover, MST1 overexpression reversed the oncogenic effects induced by circAKT3 upregulation. Nonetheless, the precise molecular mechanisms through which MST1 inhibits PCa progression warrant further investigation.

This study preliminarily explored the underlying mechanism for the observed increase in MST1 expression following the inhibition of c-Myc transcriptional activity by RPL11. It is well established that c-Myc, as a classical transcription factor, can function as both a transcriptional activator and repressor by binding to promoter regions of target genes [45, 46]. This research identified a new target gene regulated by c-Myc. Using the JASPAR database, we predicted potential c-Myc binding sites in the MST1 promoter region [27]. This interaction was subsequently validated through ChIP assays [47], which confirmed that c-Myc binds directly to the MST1 promoter, indicating that c-Myc may repress MST1 expression via this binding site.

The formation of circRNAs is a complex biological process. Numerous studies have shown that complementary sequences in the flanking introns can facilitate circRNA circularization [6, 48, 49]. In our research, we identified complementary Alu sequences within the flanking introns of circAKT3, which not only promote its circularization but also enhance the circularization of other circRNAs, such as circSOBP and circUBE3A (2,3,4,5). Prior studies have demonstrated that several classical RBPs, including MBL, QKI, and members of the hnRNP family, regulate circRNA formation [30, 50]. In this study, we found that QKI plays a regulatory role in circAKT3 formation, while FUS and hnRNPH1 did not significantly impact its circularization.

After their formation in the nucleus, circRNAs need to be transported to the cytoplasm, a process likely mediated by proteins such as URH49, exportin-2, Ran-GTP, and IGF2BP1 [7, 8]. Notably, we observed that URH49 knockdown resulted in the nuclear accumulation of circAKT3, accompanied by the suppression of MST1 expression. Here, we discovered that URH49 regulated MST1 expression through the URH49-circAKT3-RPL11-c-Myc-MST1 axis. However, the specific mechanism needs more exploration.

Conclusion

This study identified that circAKT3 was upregulated and acted as an oncogene in PCa. LNP-si-circAKT3 suppressed the growth of bone tumors formed by PCa cells. Mechanistically, circAKT3 functions as a protein scaffold by binding RPS27A and RPL11. CircAKT3 knockdown weakened their interaction, facilitated the nuclear translocation of RPL11, and enhanced RPL11-mediated inhibition of c-Myc, leading to the upregulation of

(See figure on next page.)

Fig. 8 The circularization and nuclear export of circAKT3. **A-B** Expression of circAKT3 in cells transfected with different plasmids (#1–#5). AluSc and AluSx4 sequences were deleted in the flanking introns of circAKT3 in plasmid #5. Only plasmid #1 efficiently promoted the circularization of circAKT3. Data are presented as mean ± SD. ***$P < 0.001$, ns, not significant, Student's *t*-test, $n = 3$. **C** The AluSc and AluSx4 sequences (#6) significantly promoted the biogenesis of circAKT3. Data are presented as mean ± SD. ***$P < 0.001$, Student's *t*-test, $n = 3$. **D** AluSc and AluSx4 sequences significantly promoted the circularization of circSOBP and circUBE3A(2,3,4,5). Data are presented as mean ± SD. ***$P < 0.001$, Student's *t*-test, $n = 3$. **E** Western blot analysis of URH49 expression in DU145 and PC-3 cells transfected with negative control or URH49-specific siRNA. Data are presented as mean ± SD. ***$P < 0.001$, Student's *t*-test, $n = 3$. **F** FISH images showed a significant increase in nuclear levels of circAKT3 upon URH49 downregulation. Nuclei were counterstained with DAPI. Scale bar, 20 μm. **G** CircAKT3 levels were quantitated by qRT-PCR in nuclear, cytoplasmic and total RNA extracted from DU145 (top) and PC-3 (bottom) cells treated with control or URH49-specific siRNA. Data are expressed as mean ± SD. ***$P < 0.001$, ns, not significant, Student's *t*-test, $n = 3$. **H** MST1 RNA levels were specifically downregulated following URH49 downregulation in DU145 and PC-3 cells. Data are expressed as mean ± SD. ***$P < 0.001$, *$P < 0.05$, Student's *t*-test, $n = 3$

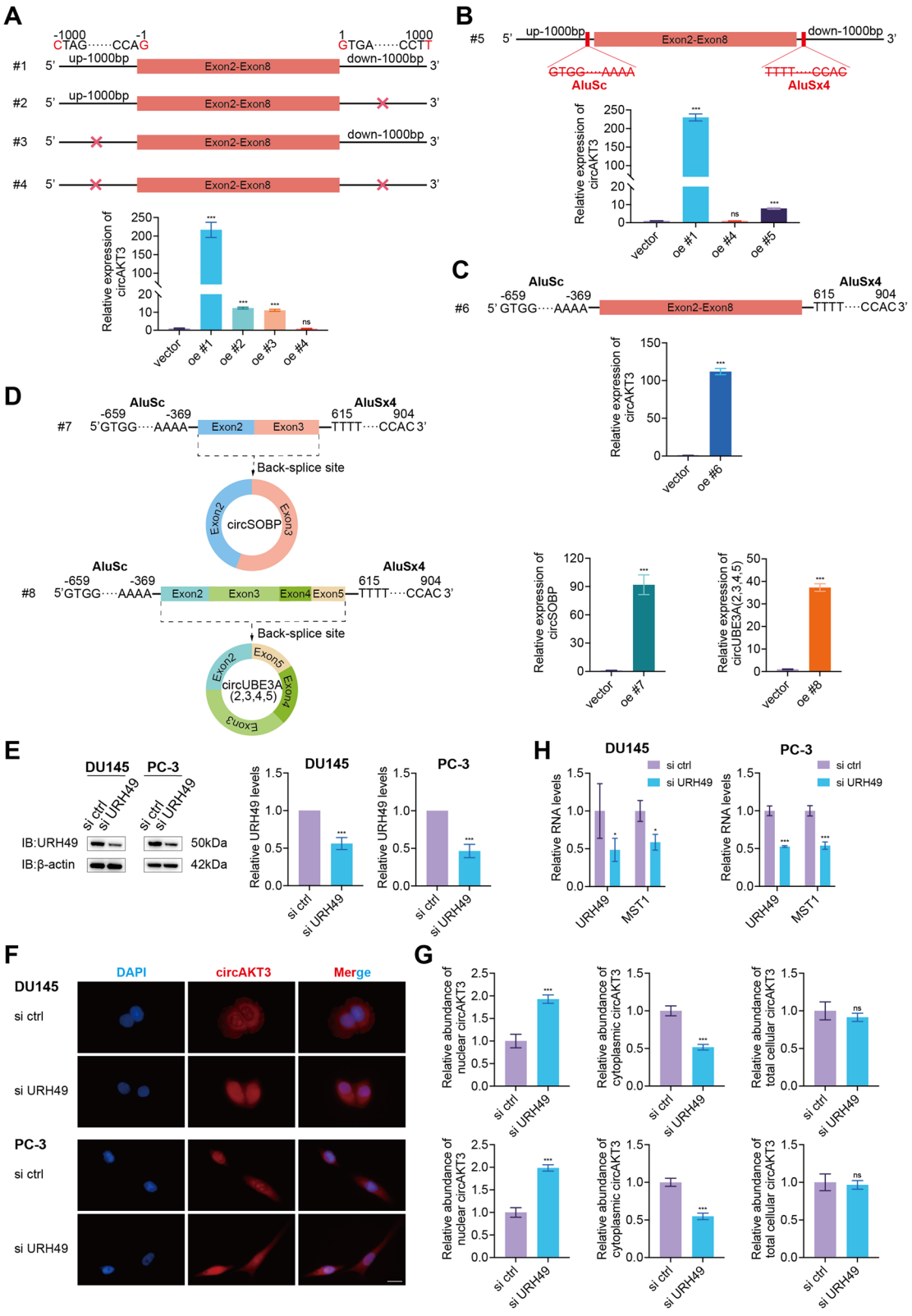

Fig. 8 (See legend on previous page.)

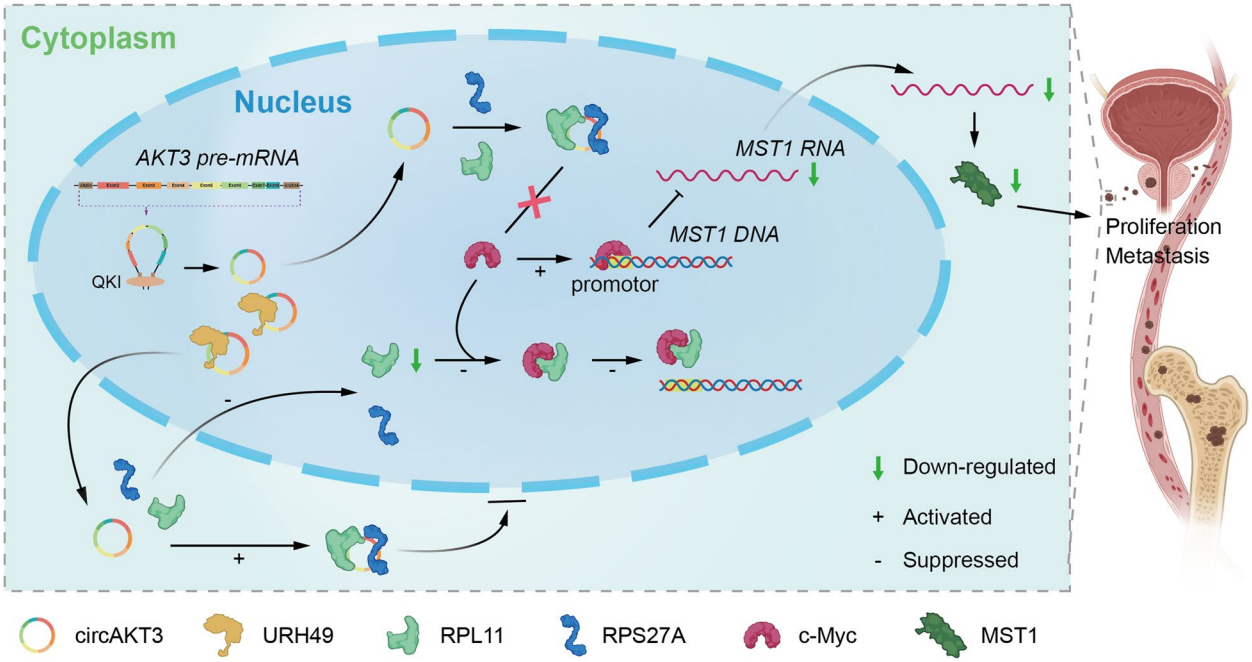

Fig. 9 Schematic Illustration of circAKT3's Role in Inhibiting PCa Proliferation and Metastasis. CircAKT3 is circularized via the involvement of flanking Alu elements and exported from the nucleus with the assistance of URH49. Serving as a molecular scaffold, circAKT3 promotes the interaction between RPS27 and ARPL11, facilitating their cytoplasmic accumulation and reducing nuclear RPL11 levels. This reduction in nuclear RPL11 diminishes its interaction with c-Myc, which in turn strengthens c-Myc-mediated suppression of MST1 expression. As a result, MST1 downregulation facilitates PCA cells proliferation and metastasis

MST1, ultimately inhibiting the proliferation, migration, and invasion of PCa cells. Additionally, both the Alu sequences and the RNA-binding protein QKI promoted circAKT3 circularization, and URH49 mediated the nuclear export of circAKT3 (Fig. 9). Our findings provide novel insights into the regulatory mechanisms of circRNAs in PCa progression and may offer potential therapeutic targets for PCa.

Supplementary Information

The online version contains supplementary material available at https://doi.org/10.1186/s12943-025-02261-6.

Supplementary Material 1.

Supplementary Material 2.

Supplementary Material 3.

Acknowledgements
We extend our gratitude to the participating physicians and patients, as well as to Dr. Jun Yan from the Department of Laboratory Animal Science at Fudan University, for his valuable review and contributions.

Authors' contributions
Xiaoming Song: Writing – original draft, Visualization, Validation, Methodology, Investigation, Formal analysis, Conceptualization. Ziwei Wei: Writing – review & editing, Validation, Methodology, Investigation, Conceptualization. Cong Zhang: Validation, Investigation. Dunsheng Han: Investigation. Jinke Liu: Investigation. Yufeng Song: Investigation. Xuefeng Xie: Investigation. Dingchang Shao: Investigation. Mingkun Zhao: Investigation. Fan Chao: Investigation. Guoxiong Xu: Writing – review & editing, Supervision, Resources, Methodology, Conceptualization. Shiyu Wang: Writing – review & editing, Supervision, Resources, Methodology, Funding acquisition, Conceptualization. Gang Chen: Writing – review & editing, Supervision, Resources, Project administration, Funding acquisition, Conceptualization. All authors have provided their consent for the publication of this manuscript.

Funding
This research was supported by the Natural Science Foundation of Shanghai (Grant No. 22ZR1409700, G.C.), the Key Specialty Construction Project at Fudan University Jinshan Hospital (Grant No. ZDXK-2024–5, G.C.), the Key Medical Specialty Construction Project in Jinshan District (Grant No. JSZK2023A03, G.C.), the National Natural Science Foundation of China (Grant No. 82303230, S.W.), and the Fundamental research program funding of Ninth People's Hospital affiliated to Shanghai Jiao Tong university School of Medicine (Grant No. JYZZ259, Z.W.).

Data availability
No datasets were generated or analysed during the current study.

Declarations

Ethics approval and consent to participate
All animal experiments were conducted in strict accordance with the *Guide for the Care and Use of Laboratory Animals* (National Institutes of Health, 8th Edition, 2011) and were approved under protocol number 2024-A021-02. The study received approval from the Ethics Committee of Jinshan Hospital, Fudan University (JIEC 2024-S19). Informed consent was obtained from all participants before their inclusion in the research.

Competing interests
The authors declare no competing interests.

Author details
[1]Department of Urology, Jinshan Hospital, Fudan University, Shanghai 201508, China. [2]Department of Urology, Shanghai Ninth People's Hospital, Shanghai Jiao Tong University School of Medicine, Shanghai 200011, China. [3]Department of Urology, Qilu Hospital of Shandong University, Jinan, Shandong 250012, China. [4]Department of Urology, Zhongshan Hospital (Xiamen Branch), Fudan University, Xiamen, Fujian 361015, China. [5]Research Center for Clinical Medicine, Jinshan Hospital, Fudan University, Shanghai 201508, China.

Received: 31 October 2024 Accepted: 6 February 2025
Published online: 25 February 2025

References

1. Siegel RL, Giaquinto AN, Jemal A. Cancer statistics, 2024. CA Cancer J Clin. 2024;74(1):12–49.
2. Teo MY, Rathkopf DE, Kantoff P. Treatment of Advanced Prostate Cancer. Annu Rev Med. 2019;70:479–99.
3. Sandhu S, Moore CM, Chiong E, et al. Prostate cancer. Lancet. 2021;398(10305):1075–90.
4. Zhu G, Chang X, Kang Y, et al. CircRNA: A novel potential strategy to treat thyroid cancer (Review). Int J Mol Med. 2021;48(5):201.
5. Liu CX, Chen LL. Circular RNAs: Characterization, cellular roles, and applications. Cell. 2022;185(13):2390.
6. Jeck WR, Sorrentino JA, Wang K, et al. Circular RNAs are abundant, conserved, and associated with ALU repeats. RNA. 2013;19(2):141–57.
7. Chen LL. The expanding regulatory mechanisms and cellular functions of circular RNAs. Nat Rev Mol Cell Biol. 2020;21(8):475–90.
8. Ngo LH, Bert AG, Dredge BK, et al. Nuclear export of circular RNA. Nature. 2024;627:212.
9. Huang C, Xu R, Zhu X, et al. m6A-modified circABCC4 promotes stemness and metastasis of prostate cancer by recruiting IGF2BP2 to increase stability of CCAR1. Cancer Gene Ther. 2023;30(10):1426–40.
10. Fang L, Du WW, Awan FM, et al. The circular RNA circ-Ccnb1 dissociates Ccnb1/Cdk1 complex suppressing cell invasion and tumorigenesis. Cancer Lett. 2019;459:216–26.
11. Lin Z, Ji Y, Zhou J, et al. Exosomal circRNAs in cancer: Implications for therapy resistance and biomarkers. Cancer Lett. 2023;566: 216245.
12. Li J, Zhang G, Liu CG, et al. The potential role of exosomal circRNAs in the tumor microenvironment: insights into cancer diagnosis and therapy. Theranostics. 2022;12(1):87–104.
13. Kristensen LS, Jakobsen T, Hager H, et al. The emerging roles of circRNAs in cancer and oncology. Nat Rev Clin Oncol. 2022;19(3):188–206.
14. Luo J, Zhao H, Chen L, et al. Multifaceted functions of RPS27a: An unconventional ribosomal protein. J Cell Physiol. 2023;238(3):485–97.
15. Wang H, Zhao J, Yang J, et al. PICT1 is critical for regulating the Rps27a-Mdm2-p53 pathway by microtubule polymerization inhibitor against cervical cancer. Biochim Biophys Acta Mol Cell Res. 2021;1868(10): 119084.
16. Wang R, Peng C, Song J, et al. Downregulated RRS1 inhibits invasion and metastasis of BT549 through RPL11-c-Myc-SNAIL axis. Int J Oncol. 2022;60(3):33.
17. Dai MS, Arnold H, Sun XX, et al. Inhibition of c-Myc activity by ribosomal protein L11. EMBO J. 2007;26(14):3332–45.
18. Dhanasekaran R, Deutzmann A, Mahauad-Fernandez WD, et al. The MYC oncogene - the grand orchestrator of cancer growth and immune evasion. Nat Rev Clin Oncol. 2022;19(1):23–36.
19. Zalcenstein A, Weisz L, Stambolsky P, et al. Repression of the MSP/MST-1 gene contributes to the antiapoptotic gain of function of mutant p53. Oncogene. 2006;25(3):359–69.
20. Wei Z, Zhang C, Song Y, et al. CircUBE3A(2,3,4,5) promotes adenylate-uridylate-rich binding factor 1 nuclear translocation to suppress prostate cancer metastasis. Cancer Lett. 2024;588: 216743.
21. Song Z, Zhuo Z, Ma Z, et al. Hsa_Circ_0001206 is downregulated and inhibits cell proliferation, migration and invasion in prostate cancer. Artif Cells Nanomed Biotechnol. 2019;47(1):2449–64.
22. Zhang C, Wang S, Chao F, et al. The short inverted repeats-induced circEXOC6B inhibits prostate cancer metastasis by enhancing the binding of RBMS1 and HuR. Mol Ther. 2023;31(6):1705–21.
23. Reymond N, D'Água BB, Ridley AJ. Crossing the endothelial barrier during metastasis. Nat Rev Cancer. 2013;13(12):858–70.
24. Li X, Wang C, Zhang H, et al. circFNDC3B Accelerates Vasculature Formation and Metastasis in Oral Squamous Cell Carcinoma. Cancer Res. 2023;83(9):1459–75.
25. Chao F, Song Z, Wang S, et al. Novel circular RNA circSOBP governs amoeboid migration through the regulation of the miR-141-3p/MYPT1/p-MLC2 axis in prostate cancer. Clin Transl Med. 2021;11(3):e360.
26. Yang M, Burton DW, Geller J, et al. The bisphosphonate olpadronate inhibits skeletal prostate cancer progression in a green fluorescent protein nude mouse model. Clin Cancer Res. 2006;12(8):2602–6.
27. Rauluseviciute I, Riudavets-Puig R, Blanc-Mathieu R, et al. JASPAR 2024: 20th anniversary of the open-access database of transcription factor binding profiles. Nucleic Acids Res. 2024;52(D1):D174–82.
28. Van der Meel R, Chen S, Zaifman J, et al. Modular Lipid Nanoparticle Platform Technology for siRNA and Lipophilic Prodrug Delivery. Small. 2021;17(37):e2103025.
29. Miao Z, Li J, Wang Y, et al. Hsa_circ_0136666 stimulates gastric cancer progression and tumor immune escape by regulating the miR-375/PRKDC Axis and PD-L1 phosphorylation. Mol Cancer. 2023;22(1):205.
30. Conn SJ, Pillman KA, Toubia J, et al. The RNA binding protein quaking regulates formation of circRNAs. Cell. 2015;160(6):1125–34.
31. Wang Q, Li Z, Yang J, et al. Loss of NEIL3 activates radiotherapy resistance in the progression of prostate cancer. Cancer Biol Med. 2021;19(8):1193–210.
32. Wang Q, Chen J, Singh S, et al. Profile of chimeric RNAs and TMPRSS2-ERG e2e4 isoform in neuroendocrine prostate cancer. Cell Biosci. 2022;12(1):153.
33. Chen L, Shan G. CircRNA in cancer: Fundamental mechanism and clinical potential. Cancer Lett. 2021;505:49–57.
34. Wen SY, Qadir J, Yang BB. Circular RNA translation: novel protein isoforms and clinical significance. Trends Mol Med. 2022;28(5):405–20.
35. Xue D, Wang H, Chen Y, et al. Circ-AKT3 inhibits clear cell renal cell carcinoma metastasis via altering miR-296-3p/E-cadherin signals. Mol Cancer. 2019;18(1):151.
36. Song J, Xu X, He S, et al. Exosomal hsa_circ_0017252 attenuates the development of gastric cancer via inhibiting macrophage M2 polarization. Hum Cell. 2022;35(5):1499–511.
37. Li H, Zhang H, Huang G, et al. Loss of RPS27a expression regulates the cell cycle, apoptosis, and proliferation via the RPL11-MDM2-p53 pathway in lung adenocarcinoma cells. J Exp Clin Cancer Res. 2022;41(1):33.
38. Abramson J, Adler J, Dunger J, et al. Accurate structure prediction of biomolecular interactions with AlphaFold 3. Nature. 2024;630(8016):493–500.
39. Zhou WY, Cai ZR, Liu J, et al. Circular RNA: metabolism, functions and interactions with proteins. Mol Cancer. 2020;19(1):172.
40. Shen H, Liu B, Xu J, et al. Circular RNAs: characteristics, biogenesis, mechanisms and functions in liver cancer. J Hematol Oncol. 2021;14(1):134.
41. Misir S, Wu N, Yang BB. Specific expression and functions of circular RNAs. Cell Death Differ. 2022;29(3):481–91.
42. Yao HP, Zhou YQ, Zhang R, et al. MSP-RON signalling in cancer: pathogenesis and therapeutic potential. Nat Rev Cancer. 2013;13(7):466–81.
43. Millar R, Kilbey A, Remak SJ, et al. The MSP-RON axis stimulates cancer cell growth in models of triple negative breast cancer. Mol Oncol. 2020;14(8):1868–80.
44. Sugie S, Mukai S, Yamasaki K, et al. Plasma macrophage-stimulating protein and hepatocyte growth factor levels are associated with prostate cancer progression. Hum Cell. 2016;29(1):22–9.
45. Patange S, Ball DA, Wan Y, et al. MYC amplifies gene expression through global changes in transcription factor dynamics. Cell Rep. 2022;38(4): 110292.
46. Kuser-Abali G, Alptekin A, Cinar B. Overexpression of MYC and EZH2 cooperates to epigenetically silence MST1 expression. Epigenetics. 2014;9(4):634–43.
47. Wang Y, Feng YC, Gan Y, et al. LncRNA MILIP links YBX1 to translational activation of Snai1 and promotes metastasis in clear cell renal cell carcinoma. J Exp Clin Cancer Res. 2022;41(1):260.
48. Zhang XO, Wang HB, Zhang Y, et al. Complementary sequence-mediated exon circularization. Cell. 2014;159(1):134–47.

49. Storer JM, Walker JA, Baker JN, et al. Framework of the Alu Subfamily Evolution in the Platyrrhine Three-Family Clade of Cebidae, Callithrichidae, and Aotidae. Genes (Basel). 2023;14(2):249.
50. Li Y, Chen B, Zhao J, et al. HNRNPL Circularizes ARHGAP35 to Produce an Oncogenic Protein. Adv Sci (Weinh). 2021;8(13):2001701.

Publisher's Note